Chapter 5

Role of dye co-adsorbent and blocking layer in improving the performance of DSSCs

This Page is intentionally left blank

5.1. Introduction

Ever growing global energy requirement and depleting level of fossil fuels have accelerated the demand for efficient power generation from solar photovoltaic (PV) cells in recent years [1-3]. The environmental impact of the use of fossil fuels is another major concern [4]. The current production of photovoltaic (PV) modules is dominated by crystalline silicon modules based on bulk wafers. However, the use of toxic materials and the high production cost of these solar cells have motivated the researchers to find new kinds of less expensive and non silicon-based solar cells to harvest solar energy efficiently [5-8].

Dye-sensitized solar cells (DSSCs) are a non-conventional photovoltaic technology that has attracted significant attention because of their high conversion efficiencies and low cost. O'Regan. B. & Grätzel reported high efficiency cells using nanoporous titanium dioxide (TiO_2) semiconductor electrodes, ruthenium (Ru) metal complex dyes, and iodine electrolyte solutions in the journal of Nature in 1991 [9]. Since then, many studies have been actively carried out on DSSCs and revealed their performance comparable to amorphous silicon thin films [10,11]. These DSSCs have the advantages of low cost, lightweight and easy fabrication, but issues include durability and further improvement of their properties. To respond to these issues, many attempts have been made, such as solidifying electrolytes and improving materials and structures, but there have been no great breakthroughs yet [12,13].

A dye-sensitized solar cell consists of two conducting glass electrodes in a sandwich arrangement. Each layer has a specific role in the cell. The transparent glass electrodes allow the light to pass through the cell. The titanium dioxide serves as a holding place for the dye and participates in electron transfer. The dye molecules collect light and produce excited electrons which cause a current in the cell. The iodide electrolyte layer acts as a source

for electron replacement. The bottom conductive layer is coated with platinum which plays the role of the counter electrode. A schematic structure of a liquid electrolyte DSSC and its working principle is shown in Fig. 5.1. When light passes through the conductive glass electrode, the dye molecules absorb the photons and the electrons in the dye go from the ground state (HOMO) to an empty excited state (LUMO). This is referred to as photoexcitation. The excited electrons jump to the conduction band of the semiconducting dioxide and diffuse across this layer reaching the conductive electrode. Then they travel through the outer circuit and reach the counter electrode. The dye molecules become oxidized after losing an electron to the semiconductor oxide material. The red-ox iodide electrolyte donates electrons to the oxidized dye molecules thereby regenerating them. When the originally lost electron reaches the counter electrode, it gives the electron back to the electrolyte [9,14].

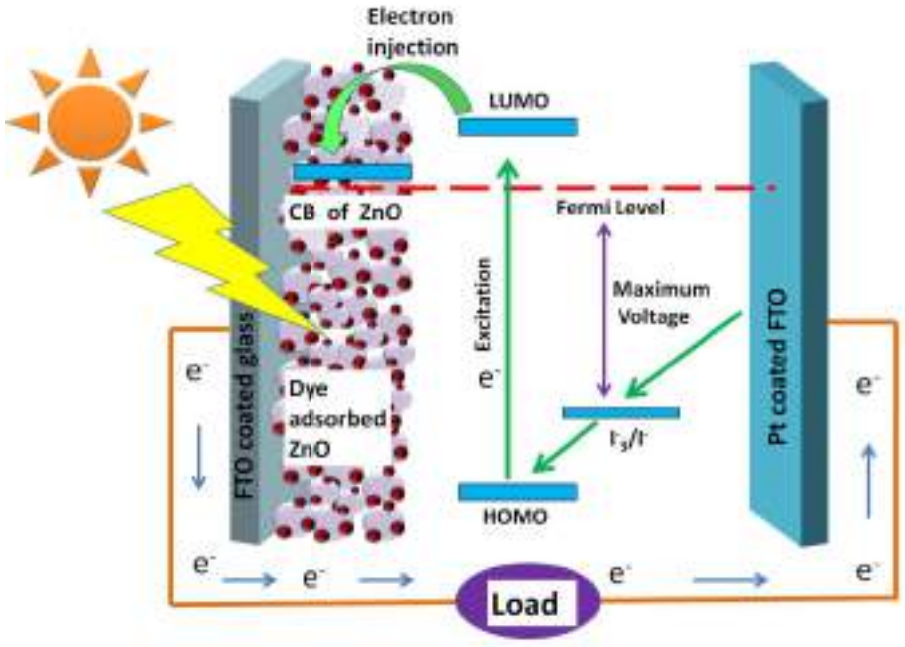

Figure 5.1 Schematic diagram and working principle of a conventional DSSC.

The photovoltaic performance of a DSSC highly depends on all of its components and the fabrication methodology. Therefore, the optimization of every component is extremely crucial to achieve the best performance. Since its

introduction into the science community in 1991, the nanocrystalline photoanode in dye-sensitized solar cells has predominantly been comprised of titanium (TiO_2) nanoparticles as the semiconducting material [9,14,15]. Many researchers became very interested in studying the dye-sensitized solar cell performance fabricated using alternative semiconducting nanomaterials [16,17]. Specifically, Zinc Oxide (ZnO) has been an ideal alternative to TiO_2 because of having a similar conduction band edge that is appropriate for proper electron injection from the excited dyes; moreover, ZnO provides better electron transport due to its higher electronic mobility. Along with that, ZnO is also highly transparent, which allows greater light penetration [18-22].

In this study, ZnO nanoparticles were implemented to fabricate the photoanode of the DSSCs and rose bengal dye was utilized as a sensitizer. To obtain better efficiency, the dye molecules must bind tightly to the mesoporous ZnO photoanode surface with the assistance of their anchoring group to ensure proficient electron injection from the LUMO of the dye molecule to the conduction band (CB) of ZnO.

Ruthenium dyes have long been used as quite efficient sensitizers for the photoanodes of the DSSCs [23-25]. However, these dyes are expensive, difficult to synthesis, requires high production cost, toxic, rare and easily pollute the environment [26]. Owing to these facts, the organic photosensitizer Rose Bengal (RB), emerges as a promising and alternative candidate. It is a xanthenes class photosensitizer having high absorbtion coefficient and absorbs a wide spectrum of solar radiation. It energetically matches the conduction band edge of ZnO and iodine/iodide redox couple for DSSC application [27,28]. Accordingly, ZnO based DSSC performes specifically well when sensitized with Rose Bengal. Although the efficiency of these type of organic sensitizer based DSSCs is less, production cost per watt will be less compared to the ruthenium based DSSCs even if we achieve moderate efficiency. As the RB dye is an organic dye and does not contain any toxic noble metal such as

ruthenium, there are no environmental pollution related issues with it. It is widely used because of its high absorption coefficient in the visible region of solar spectrum and its molecular structure (Fig. 5.2.) comprises of anchoring groups that can be adsorbed onto the semiconductor oxide surface. For the particular case of ZnO-RB combination, the interaction between the unfilled valance shell of the ZnO and the carboxyl groups present in the dye molecules leads to easy adsorption of the dye molecules on the ZnO surface. Such kind of bonding between the dye molecule and ZnO not only increases adsorptivity of dye but also facilitates electron injection because of the substantial overlap between the electron molecular orbitals of the dye and those of the semiconductor's conduction band [29].

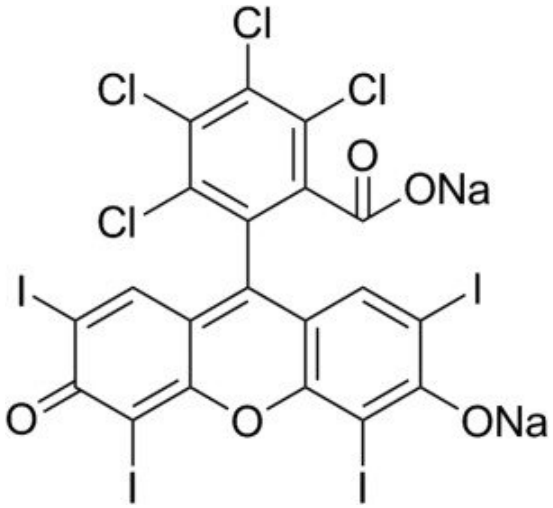

Figure 5.2 Chemical structure of Rose Bengal dye.

However, in case of ZnO photoanode based DSSCs, the dye aggregation on the ZnO surface affects the photoelectron injection by increasing charge recombination and hence limits the overall device performance [30-32. The use of additives such as Chenodeoxycholic acid (CDCA) is a very useful and widely used strategy in lowering the self-aggregation of dye molecules by suppressing unfavourable dye-dye interactions as shown in Fig. 5.3 and thereby enhances the photoconversion efficiency [33-

35]. However, the strong binding of CDCA molecules to the ZnO surface partially displaces dye molecules and consequently reduces photon harvesting. Therefore, to maximize the positive effect of the co-adsorbent, it is very crucial to carefully optimize the amount of CDCA [36]. Few researchers have studied the role of CDCA as an anti-aggregation agent in ruthenium and organic dye based DSSCs and found it to be very effective in reducing the aggregation of dye molecules over the semiconductor surface [37-40]. But there is no report available related to the application of CDCA on Rose Bengal dye. Herein, we report the investigation on the effect of CDCA as co-adsorbent in the performance of Rose Bengal (RB) dye based DSSCs. Different concentrations of CDCA were studied to identify the optimum value for achieving the best device performance.

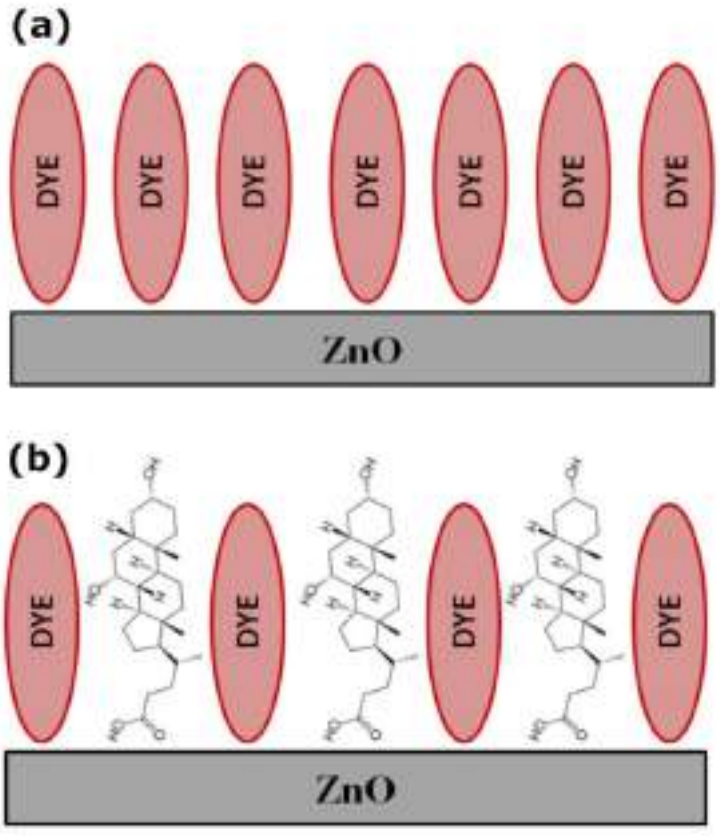

Figure 5.3 (a) Unfavourable dye-dye interaction in absence of CDCA (b) reduced self-aggregation of dye molecules in presence of CDCA.

On the other hand, the mesoporous nature of the ZnO film is very essential to tender high surface area offering more dye loading and thereby generating more photoelectrons. However, small pores present in the nanocrystalline ZnO layer of the photoanode may provide a path for the direct contact between the liquid electrolyte and the FTO substrate. This may allow the electrons of FTO to recombine with the I^-_3 ion present in the electrolyte resulting in high recombination current and hence decreased cell performance [41,42]. Therefore, to inhibit the electron back transfer, a promising approach is to modify the FTO/electrolyte interface by adding a compact metal oxide blocking layer. A thin blocking layer (BL) of ZnO was deposited by a facile and cost-effective sol-gel spin coating process before depositing the mesoporous active ZnO layer. In this work, we reported the fabrication and characterization of DSSCs based on ZnO nanoparticles and Rose Bengal dye. The effect of CDCA concentration and the compact ZnO blocking layer in boosting the photovoltaic performance of the device was investigated in terms of photocurrent-voltage (J-V) characteristics and dark current measurement. In addition to that, electrochemical impedance spectroscopy (EIS) analysis was employed to investigate the charge transfer kinetics and electron back reaction of the fabricated cells.

5.2. Materials and Methods

5.2.1. Materials

ZnO nanopowder, Zinc acetate dehydrate $(CH_3COO)_2Zn$, $2H_2O$) and Monoethanolamine (MEA) were bought from Sigma Aldrich, India. ethylcellulose and terpineol were bought from TCI Chemicals, India. Transparent FTO coated glass (10 Ω/ square), the high-performance liquid electrolyte (Iodolyte AN50), chenodeoxycholic acid (CDCA) as a dye co-adsorbent and liquid platinum paint (Platisol T) to prepare the platinum-coated counter electrode were purchased from Solaronix, Switzerland. Meltonix 1170-

25 (25µm) (Solaronix) was used as a spacer between the working and counter electrode to avoid short-circuiting. All the reagents utilized in the fabrication process were of analytical grades. So no further purification was required.

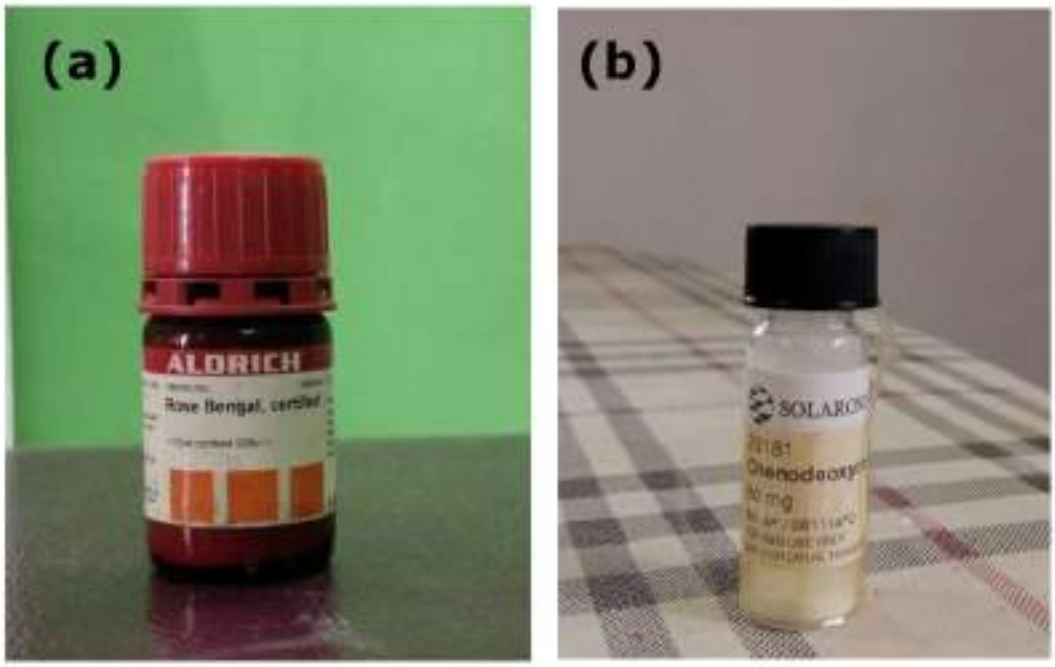

Figure 5.4 (a) Rose Bengal dye and (b) chenodeoxycholic acid (CDCA).

5.2.2. Preparation of conventional ZnO photoanode

To prepare the thin films of the photoanode materials, the FTO coated glass substrates were first cleaned with dilute HCl in an ultrasonic bath for 15 minutes and then thoroughly rinsed with deionized water to remove the HCL residues. The substrates were then cleaned with acetone and ethanol using an ultrasonic cleaning bath [17,22]. The mesoporous ZnO photoelectrode of the DSSC was prepared by following the standard doctor blade method. The paste for doctor blading was prepared by mixing 0.5 g of ZnO nanopowder with α-terpineol as a solvent and 0.45 g of ethyl cellulose as a binder [43]. The mixture was stirred continuously to obtain a smooth lump-free slurry. The ZnO paste was then coated on the conductive side of the cleaned FTO glass

substrate and subsequently annealed at 400^{o}C on a hot plate for 30 min to burn out the ethyl cellulose and other organic contents of the working electrode and to strengthening the bonding between the substrate and the ZnO film. In addition to that, the annealing procedure also helps to improve the surface quality of the thin film along with increasing the crystallinity of the sample [44-47].

5.2.3. Preparation of photoanode with Compact ZnO layer

In order to improve the photovoltaic performance of the cells further by preventing the direct contact between FTO and liquid electrolyte, a thin and compact ZnO layer was deposited on FTO coated glass substrate by employing a simple sol-gel spin coating method prior to deposition of mesoporous active ZnO nanoparticle layer. The precursor solution was prepared by mixing Zinc acetate dehydrate $(CH_3COO)_2Zn$, $2H_2O$) in 50 ml isopropanol as solvent and monoethanolamine (MEA) was used as a stabilizer. The precursor solution concentration was maintained at 0.05 M. The mixture was vigorously stirred at 60° C by a magnetic stirrer for 1 hr. MEA was added dropwise under stirring, yielding a clear homogenous solution. The solution was left for 24 hr at room temperature for aging before it could be used for film deposition. The aged solution was then spin-coated on a cleaned FTO glass substrate with a programmable spin coater (Apex Instruments Co. Pvt. Ltd, Model SpinNXG-P1) at 3000 rpm for 30 s and annealed at 200° C for 20 minutes to form the ZnO blocking layer. Over this compact blocking layer, the mesoporous active layer was coated using the same doctor blade method and then annealed at 400° C as done earlier.

5.2.4. Assembling the devices

One set of ZnO photoanodes were sensitized by immersing them in a 0.5 mM ethanolic solution of pure Rose Bengal dye for 12 hours. Another set of

photoanodes (both with and without ZnO blocking layer) were sensitized with the RB dye solution containing various concentrations (0 mM – 10 mM) of CDCA at room temperature for 12 hours. The working electrodes were then removed from the solution and rinsed thoroughly with deionized water and ethanol to get rid of any excess dye from the thin film surface and left for air drying at room temperature. The platinum catalyst precursor solution (Platisol-T) was spin-coated on the conducting side of the cleaned FTO glasses and heated at 450^{o} C for 15 minutes on a hot plate to prepare the counter electrodes for the cells. The dye adsorbed working electrodes and platinum(Pt)-coated counter electrodes were assembled against the coated sides of each other in a sandwich manner using two binder clips with a Surlyn film (Meltonix 1170-25µm, Solaronix) gasket as a spacer in between them. The liquid electrolyte used in the fabrication process was poured inside the cell through fine holes pre-drilled on the counter electrodes. The red-ox concentration of the electrolyte was 50 mM. The active area of the cells for illumination was adjusted to 0.16 cm^2.

5.2.5. Characterization and Measurements

X-ray diffraction (XRD) analysis is a technique used for the determination of the crystal structure of materials in the nanomaterial, thin-film, or bulk material form. In the XRD experiment, a monochromatic X-ray beam is allowed to incident on the sample and the diffraction occurs. In our study, the X-ray diffraction analysis was employed using PAN-analytical X'Pert PRO X-ray diffractometer (CuKα radiation, 30 mA, 40 kV, λ= 1.5406 Å) to determine the crystalline structure of ZnO nanoparticles used in making the photoanode of the DSSC. Absorbance spectrum measurement of the dye was carried out using a Perkin-Elmer Lambda-35 UV-VIS spectrophotometer. Scanning electron microscopy (JEOL) was used to examine the surface morphology of the prepared ZnO thin films. The current-voltage (J-V)

characterization of the cells was measured under 100 mW/cm^2 illumination using a Keithley 2400 digital source meter which was controlled by Keithley LabTracer computer software. The overall photoconversion efficiency of the solar cell was calculated using the formula

$$\eta = \frac{P_{out}}{P_{in}} = \frac{I_{sc}V_{oc}FF}{P_{in}} \qquad (1)$$

Where $P_{in,}$ V_{oc}, I_{sc} and FF denote the incident photon power, open-circuit voltage, the short circuit current density and fill factor respectively. The fill factor was estimated using the following formula:

$$FF = \frac{I_{max}V_{max}}{I_{sc}V_{oc}} \qquad (2)$$

Where I_{max} and V_{max}, respectively, represent values of current and voltage at the maximum output power point of the solar cell. The area of the fabricated cells that was exposed to light was 1 cm^2. The electrochemical impedance spectroscopy (EIS) of the cells was done in the frequency range of 0.1Hz to 190 kHz under open circuit conditions.

5.3. Results and Discussion

5.3.1. UV-VIS absorption spectral analysis of the dye

0.5 mM ethanolic solution of Rose Bengal dye was prepared and its absorption property was studied using Perkin Elmer Lambda–35 UV-VIS spectrophotometer. UV-VIS absorption spectrum of the RB dye is shown in Fig. 5.6 (b). The value of λ_{max} obtained from the absorption spectrum is a very important parameter as it demonstrates the potential of the molecular systems for significant usage as a functional material in DSSC. It can observed that the Rose Bengal dye absorbs a larger fraction of the solar spectrum in the visible region of 460–600 nm and it shows the highest optical absorption at 549 nm wavelength. The strong absorption peak may be assigned to the intra-molecular

charge transfer (ICT) transitions from the donor to acceptor level within HOMO (Highest Occupied Molecular Orbital)- (Lowest Unoccupied Molecular Orbital)LUMO energy levels as shown in Fig.5.5 [48].

Figure 5.5 Possible transition mechanism in the Rose Bengal molecular system.

The optical energy gap of the dye was calculated to be 2.26 eV from the absorption spectra using equation (3) given below [49] (Ossai et al 2020).

$$E_g = \frac{1240}{\lambda_{max}}\ eV \qquad (3)$$

where λ_{max} is the maximum absorption wavelength.

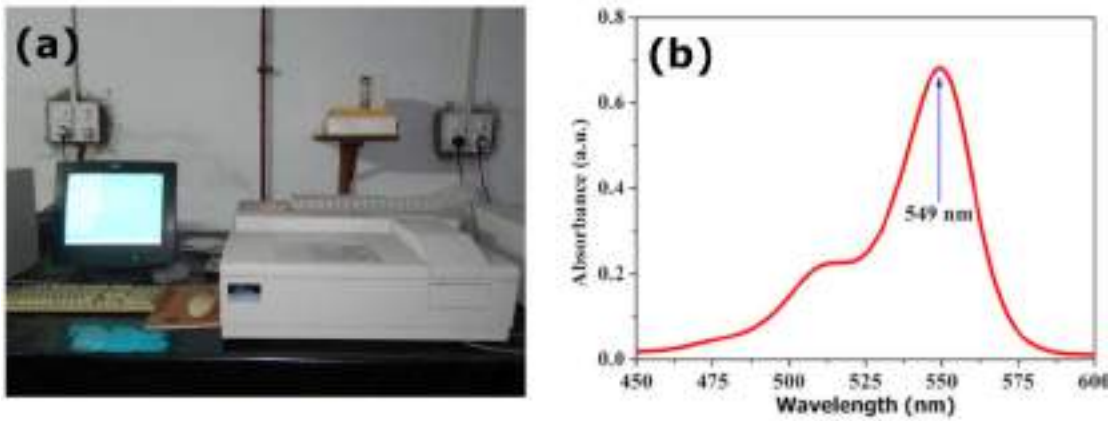

Figure 5.6 (a) UV-VIS experimental setup (b) absorption spectra of Rose Bengal dye.

The dye's HOMO-LUMO energy gap has an impact on how electrons are injected into the ZnO particles' conduction band from the dye's LUMO molecule. It facilitates the vertical electron transition through the dye excitation [50]. On the other hand, indirect transition is a phonon assited transition where change in momentum must be taken into account. When the photons having energy fairly above the indirect band gap of dye molecule is absorbed by the dye electron, phonons get emitted [51]. As a result the direct band gap is utilized to determine the vertical transition during the course of photosesitization [52,53]. Hence, the lowest electronic transition, which corresponds to the onset of absorption in the UV-visible absorption spectrum, was used to calculate the optical bandgap. It is the energy difference between HOMO and LUMO which is caused by the excitation of electrons from HOMO to LUMO.

5.3.2. Structural and phase characterization ZnO compact layer

The X-ray diffraction pattern of the ZnO compact blocking layer, shown in Fig. 5.7 (a), exhibits the hexagonal wurtzite crystal phase of ZnO and the peaks well match with the standard JCPDS card no. 36-1451. The diffraction peaks observed at 2θ values of 31.79°, 34.42°, 36.25°, 47.51°, 56.60°, 62.86°, 67.96°, and 69°corresponds to the reflection from the (100), (002), (101), (110), (103), (112), and (201) lattice planes respectively. Sharp and strong peaks indicate the highly crystalline nature of the material [54,55]. The XRD pattern for the commercial ZnO nanopowder is shown in Fig. 5.7 (b). It can be clearly seen that both the commercial ZnO nanopowder and synthesized ZnO blocking layer showed similar XRD patterns. The XRD pattern of sample with both the blocking and active layer is shown in Fig. 5.7 (c). This is very similar to the XRD pattern of the blocking layer. This is because the blocking layer is more crystalline in nature, which is evident from its XRD pattern with its sharper peaks.

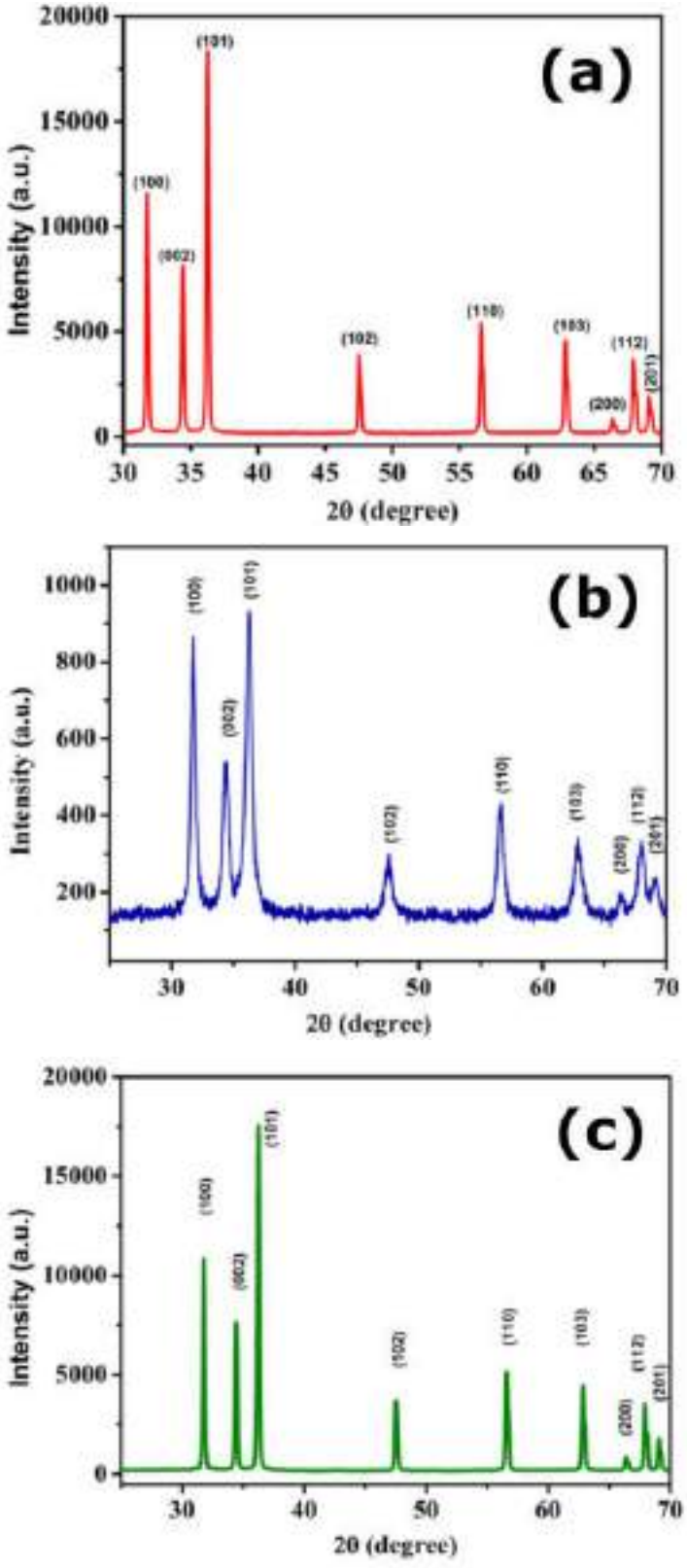

Figure 5.7 X-ray diffraction pattern of (a) ZnO compact blocking layer (b) ZnO nanoparticles as active layer (c) ZnO blocking/active layer.

5.3.3. Surface Morphology study and energy dispersive spectroscopy of the photoanodes

Scanning electron microscopic (SEM) analysis of the ZnO active layer and the compact blocking layer on the FTO substrate was carried out to study the surface morphology and the particle size of the sample. The SEM images of the ZnO active and blocking layers on the FTO substrate are depicted in Fig. 5.8 and Fig. 5.9 respectively. It can be seen from Fig. 5.8 (a) that the ZnO nanoparticles have a hexagonal structure. Fig. 5.9 (a) and 5.8 (b) represent the SEM images of compact blocking layer at low and high magnifications respectively. The diameter of the spin-coated nanoparticles ranges from 150 to 180 nm. Further, the chemical composition and elemental percentage of the compact ZnO film are revealed by the Energy Dispersive X-Ray Spectroscopy (EDS) analysis which is shown in Fig. 5.10. Predominating peaks of Zn and O_2 unveil that the synthesized blocking layer contains pure ZnO.

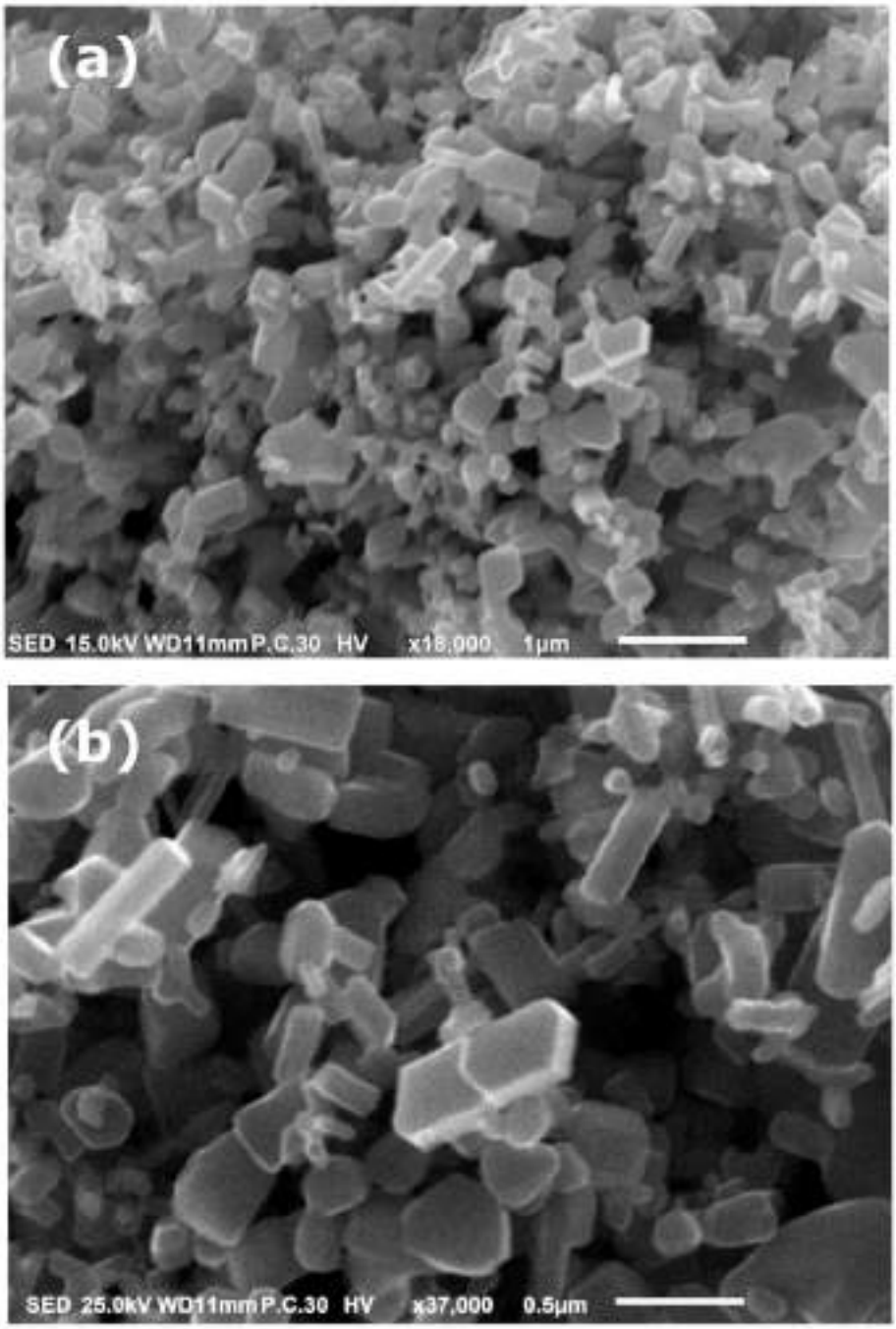

Figure 5.8 SEM images of ZnO NP active layer (a) at lower magnification (b) at higher magnification.

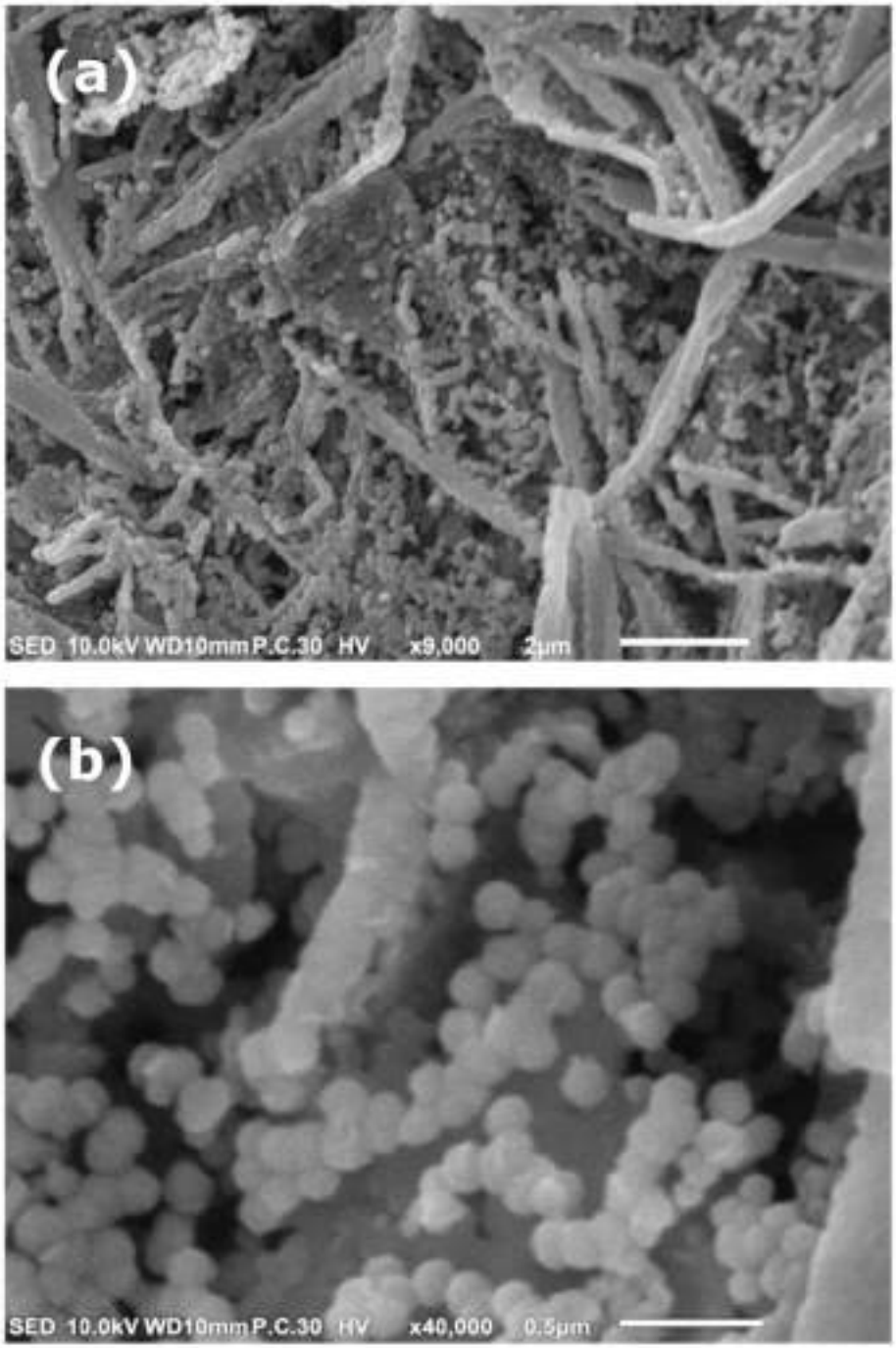

Figure 5.9 SEM images of ZnO blocking layer (a) at lower magnification and (b) at higher magnification.

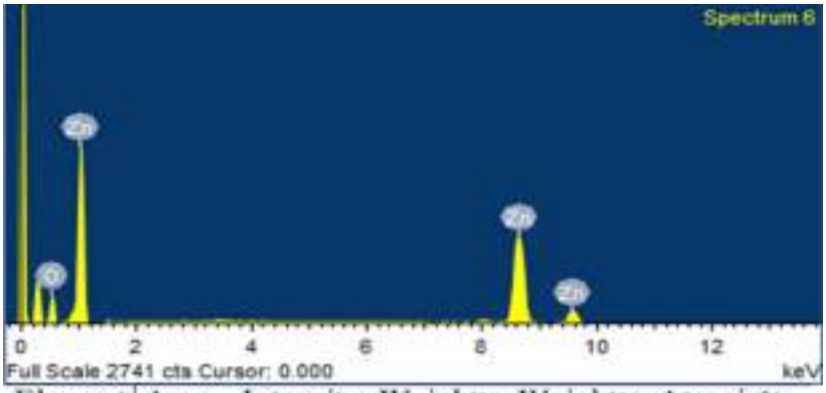

Element	App Conc.	Intensity Corrn.	Weight%	Weight% Sigma	Atomic%
O K	9.18	0.8566	16.72	0.73	45.06
Zn K	51.11	0.9578	83.28	0.73	54.94
Totals			100.00		

Figure 5.10 EDS and elemental composition of ZnO blocking layer.

5.3.4. Photovoltaic characterization of the cells

The Current-Voltage (J-V) characteristic is a crucial measurement that reveals the value of the overall photovoltaic performance of a solar cell along with the key performance parameters like open circuit voltage and short circuit current density. Fig. 5.11 (a) depicts the J-V characteristics of the DSSCs based on different types of photoanodes under illumination and the obtained photovoltaic parameters for each of the cells are summarized in Table 5.1.

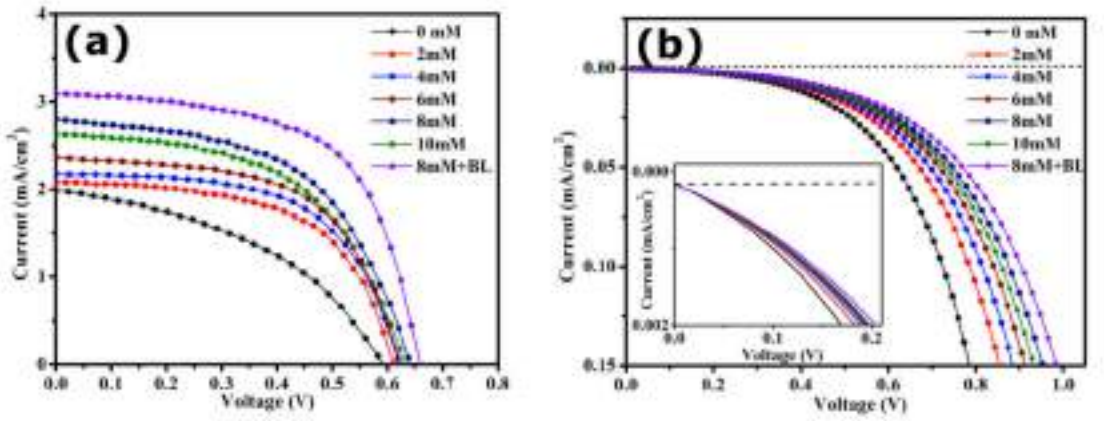

Figure 5.11 Current-voltage characteristics of different cells under (a) illumination (b) dark

Table 5.1.

Photovoltaic parameters of DSSCs fabricated with various ZnO photoanodes

Cell name	CDCA concentration	J_{sc} (mA/cm^2)	V_{oc}(V)	FF	Efficiency (η %)
DSSC1	0 mM	1.98	0.58	0.43	0.49
DSSC2	2 mM	2.08	0.61	0.58	0.74
DSSC3	4 mM	2.18	0.62	0.60	0.81
DSSC4	6 mM	2.36	0.63	0.58	0.86
DSSC5	8 mM	2.80	0.64	0.56	1.00
DSSC6	10 mM	2.63	0.64	0.54	0.91
DSSC7	8 mM + BL	3.09	0.66	0.60	1.22

5.3.5. Effect of CDCA

The conventionally prepared DSSC with ZnO nanoparticles and Rose Bengal dye displayed a short circuit current density (J_{sc}) of 1.98 mA/cm^2, an open circuit voltage (V_{oc}) of 0.58 V, and a fill factor (FF) of 0.43, resulting in a photoconversion efficiency (η) of 0.49 %. However, under the same working conditions, the device performance was found to be highly influenced when CDCA solution was incorporated into the dye solution at various concentrations. From Table 5.1, it can be noted that the value of V_{oc}, as well as J_{sc}, increases with an increase in the concentration of CDCA. Optimum concentration (8mM) provides the finest dye attachment to the ZnO surface. The best device performance was achieved for the optimized CDCA concentration of 8 mM when added with 0.5 mM RB dye solution. This improvement in the performance may be attributed to reduced dye aggregation along with uniform dye adsorption yielding better electron injection into the conduction band of ZnO.

5.3.6. *Effect of compact ZnO blocking layer*

To avoid the direct contact between the FTO and the liquid electrolyte through the pores present in the nanocrystalline ZnO film in a conventionally prepared DSSC, a thin and compact layer of ZnO was employed as shown in Fig. 5.12. From Table 5.1 it can be observed that the addition of a compact ZnO blocking layer in DSSC7 with 8 mM CDCA additive shows a remarkable enhancement in J_{sc} (3.09 mA/cm^2) and V_{oc} (0.66 V) and consequently the highest value of photoconversion efficiency η (1.22 %) was obtained among all the fabricated cells. Such type of performance enhancement may be accredited to the consolidated effect of improved dye loading due to the addition of CDCA with proper concentration and increased charge collection along with decreased electron recombination at the FTO/ZnO/electrolyte interface hindering the direct contact between FTO and electrolyte by the blocking layer.

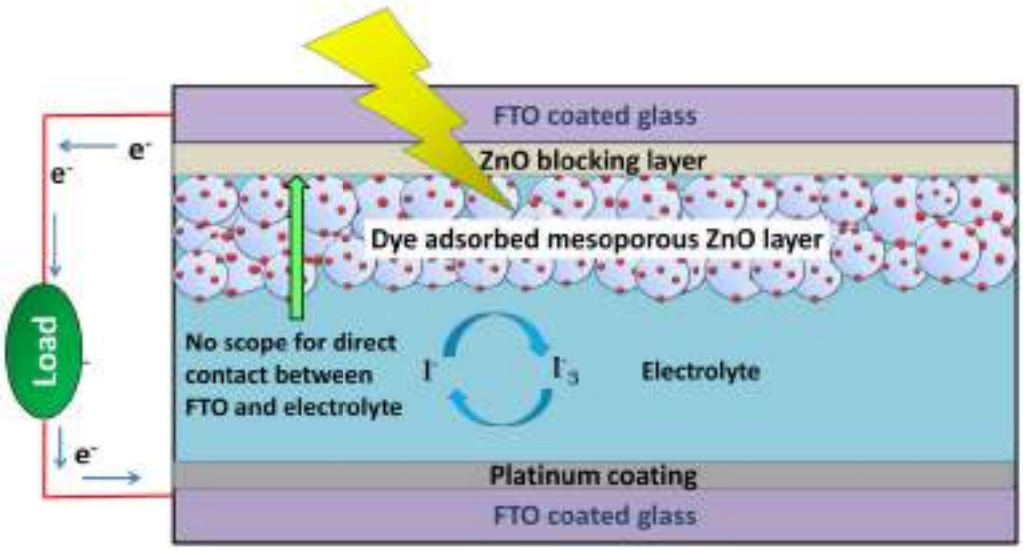

Figure 5.12 Schematic diagram of a DSSC with compact ZnO blocking layer.

5.3.7. *Dark current measurement*

To explore the effect of CDCA concentration and ZnO blocking layer in the process of electron back transfer, the J-V characteristics were also

measured in the dark which is shown in Fig. 5.11(b). It is regarded as a qualitative method to assess the degree of electron back transfer in DSSCs. The dark current generation is known to be partly due to the presence of exposed FTO sites having direct contact with the liquid electrolyte and the pores left between the ZnO nanoparticles and the FTO surface [41,42]. These exposed FTO sites and the pores of ZnO nanoparticle film would allow the liquid electrolyte to penetrate through ZnO film and directly come in contact with bare FTO sites resulting in recombination losses as shown in the energy band diagram for conventional ZnO NP based DSSC in Fig. 5.13(a). It can be observed from Fig. 5.11(b) that for a particular value of the voltage on the X-axis (i.e. voltage axis) of the dark current characteristics, the corresponding Y-axis value (i.e. value of dark current) is lowest for DSSC7 for that particular voltage. It can also be seen that the dark current has the highest value for conventionally prepared cell (DSSC1) with bare FTO and decreases with an increase in CDCA concentration up to 8 mM. An enlarged plot of the dark current characteristics is provided as an inset in Fig. 5.11(b) so that a clear scenario is observed. For the cell (DSSC7) with compact ZnO BL and 8 mM CDCA solution as dye co-adsorbent, the dark current is reduced significantly for the same bias potential in comparison to all other cells. This demonstrates that the compact ZnO BL reduces the bare FTO site and thereby successfully suppresses the dark current by lowering the electron back transfer. It was also observed that the DSSC7 has the slowest rate of increase of dark current with an increase in bias voltage confirming excellent suppression of electron recombination and consequently reduced current loss.

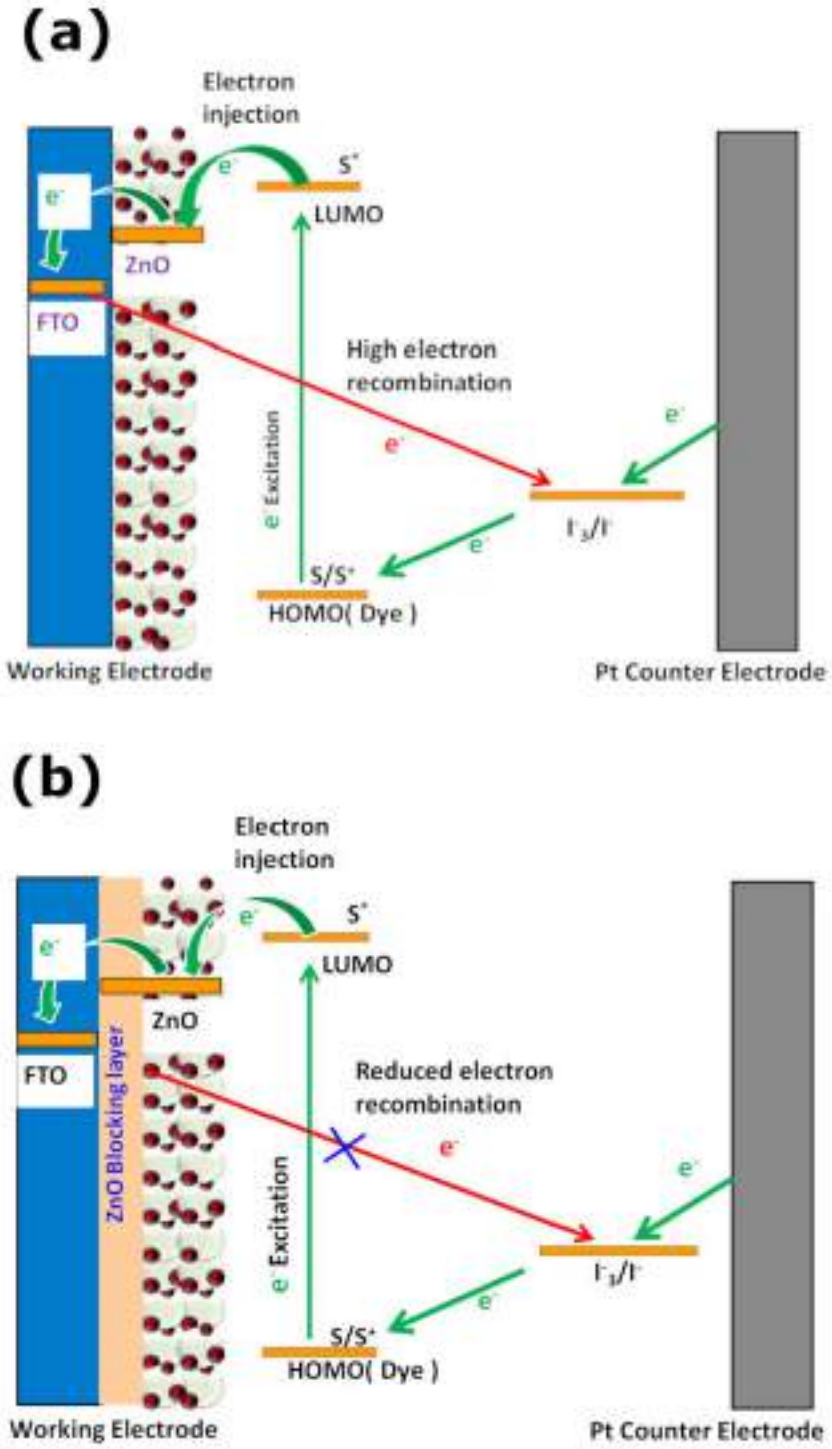

Figure 5.13 Schematic diagram showing interfacial charge transfer and recombination in case of DSSCs (a) without ZnO BL (b) with compact ZnO BL.

The variations of different cell parameters with the concentration of CDCA solution for the fabricated DSSCs are depicted in Fig. 5.14. It can be observed that CDCA concentration highly influences the value of J_{sc}. ZnO BL improves the current further. A small increase in the values of V_{oc} and FF can also be noted from Fig. 5.11 due to these processes. The highest values of cell parameters were obtained for the cell DSSC7.

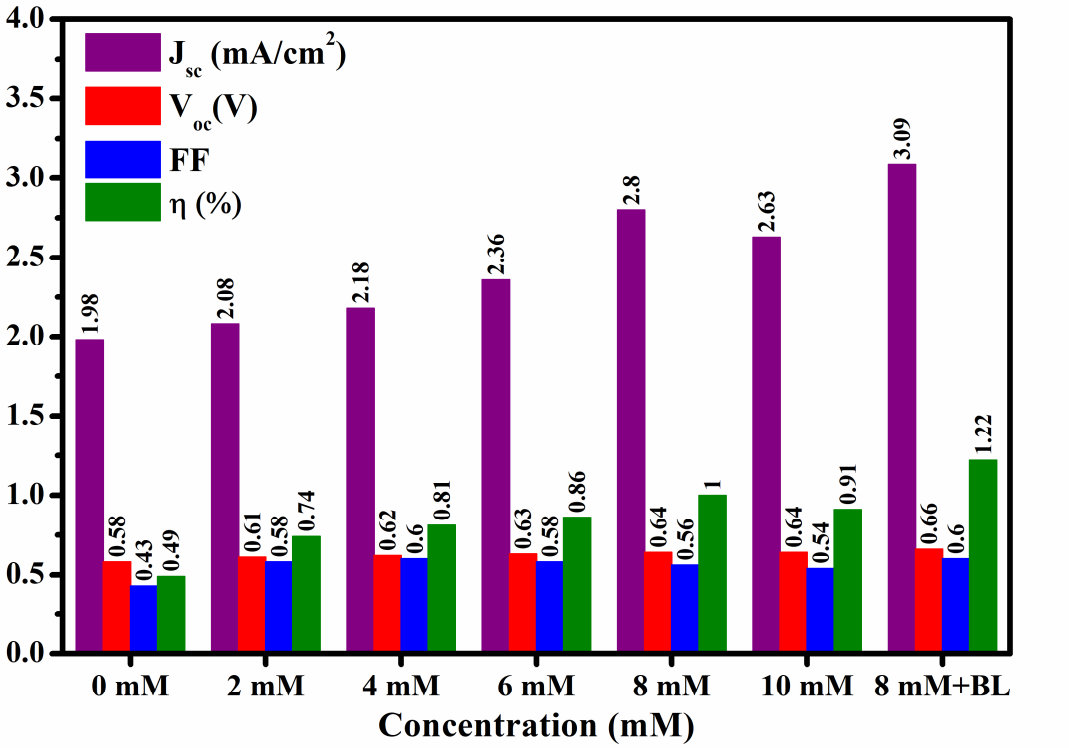

Figure 5.14 Effect of CDCA concentration and ZnO blocking layer (BL) on different cell parameters.

5.3.8. Electrochemical impedance spectroscopy study

To further gain an insight into the influence of CDCA concentration and the coating of compact ZnO blocking layer on the charge transfer and recombination kinetics of the prepared devices, the DSSCs were further investigated by electrochemical impedance spectroscopic (EIS) measurement in dark under V_{oc} bias voltage with 10 mV AC perturbation amplitude. This

gives a more precise understanding of the limiting factors for the cell performance parameters. In the EIS measurement done under the dark condition and with an applied bias voltage, electrons from FTO are injected into the conduction band of ZnO and then transported through the ZnO network. Some of the injected electrons recombine with the I_3^- ion present in the electrolyte giving rise to the recombination phenomenon [56]. Fig. 5.14(a) shows the Nyquist plot of all the prepared cells exhibiting two obvious semicircles. The curves are fitted using the equivalent circuit shown in the inset of Fig. 5.15(a) and the EIS measurement results obtained in terms of resistances and capacitances are summarized in Table 5.2. The charge transfer resistance (R_{pt}) and double layer capacitance (C_{pt}) at the Pt counter electrode/electrolyte interface is responsible for the first semicircle in the high-frequency range, while the second semicircle in the mid-frequency range may be assigned to the charge transfer and recombination resistance (R_{rec}) and chemical capacitance (C) at the ZnO/dye/electrolyte interface [36,57,58]. The intercept at the real axis of the Nyquist plot represents the series resistance (R_s) of FTO and other ohmic contacts like connecting cables, clamps and clips used to connect the cells for measurement. [59,60].

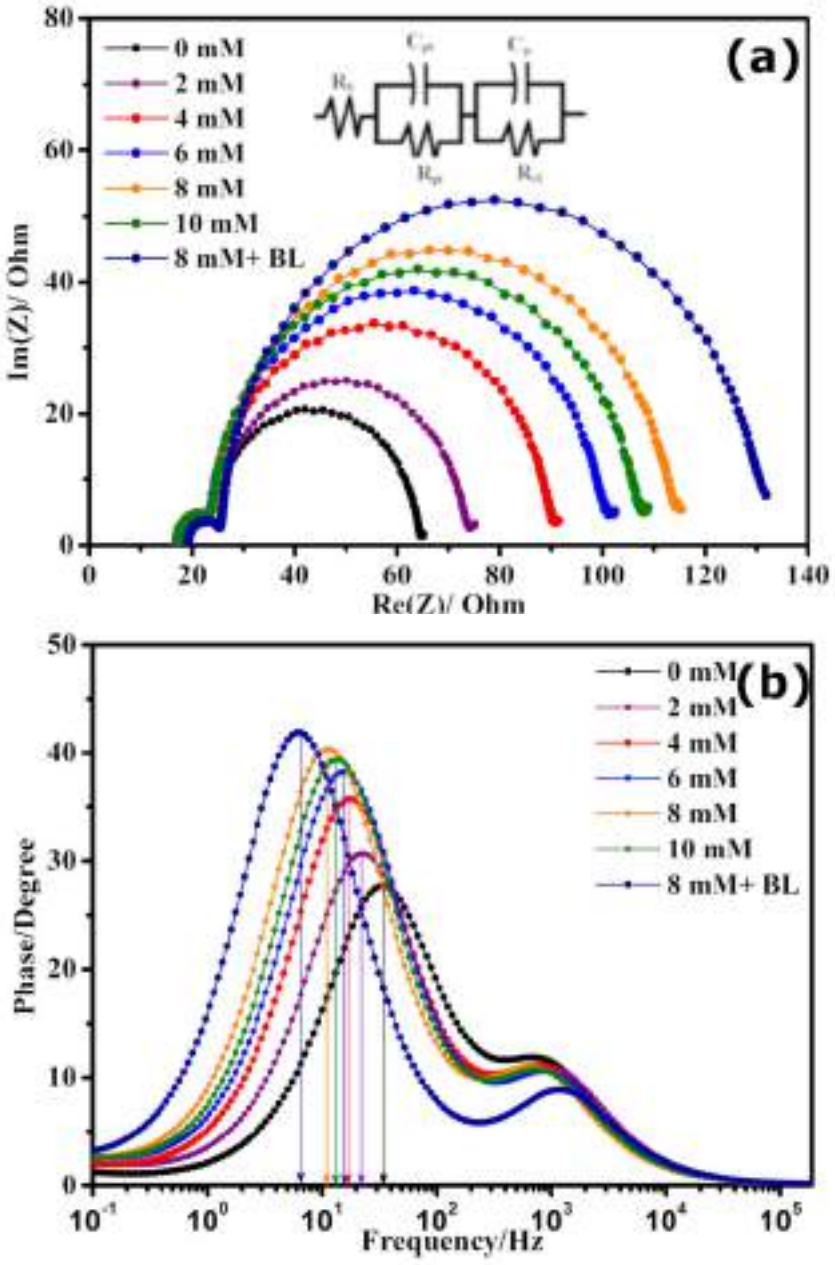

Figure 5.15 EIS of the DSSCs representing (a) Nyquist plot along with equivalent circuit (inset) and (b) Bode plot.

Table 5.2 Summary of EIS measurement.

Cell name	CDCA concentration	R_s (Ω)	R_{pt} (Ω)	R_{rec} (Ω)	Peak freq. f(Hz)	Electron lifetime (τ_e) (ms)
DSSC1	0 mM	17.15	6.51	40.2	34.21	4.65
DSSC2	2 mM	17.23	6.55	48.8	22.13	7.19
DSSC3	4 mM	17.05	6.46	65.4	17.05	9.34
DSSC4	6 mM	17.12	6.23	75.2	15.62	10.94
DSSC5	8 mM	17.36	6.65	87.6	11.03	14.45
DSSC6	10 mM	17.29	6.37	81.4	13.13	12.13
DSSC7	8 mM + BL	19.23	6.39	102.7	6.54	24.35

The small semicircles in the high-frequency range are almost identical indicating nearly similar values of R_{pt} for all four kinds of cells as all of them have similar Pt counter electrodes and the same electrolyte. On the contrary, a substantial dissimilarity can be observed in large semicircles in the mid-frequency range. This indicates that the charge transport and recombination behaviour at the ZnO/dye/electrolyte interface was extensively affected due to working electrode modification by the addition of CDCA and incorporation of the blocking layer. The middle arc of the Nyquist plot for the conventionally prepared DSSC has the lowest diameter indicating the lowest recombination resistance (R_{rec}) and thus representing the highest recombination process among all the cells. The diameter is evidently larger for the CDCA treated cells indicating its positive role in increasing the recombination resistance and hence lowering the recombination phenomena. It can be observed from Table 5.2 that the recombination resistance increases in the order of DSSC1 < DSSC2 <

DSSC3< DSSC4< DSSC6 < DSSC5< DSSC7 indicating that the recombination resistance increases with an increase in CDCA concentration from 0 to 8 mM and decreases at 10 mM concentration. The larger R_{rec} value indicates it is more difficult to transfer the injected electrons from the ZnO back to the electrolyte, and thus the back recombination can be suppressed in the cell, thus giving a higher J_{sc} and V_{oc}. The highest value of recombination resistance is obtained when the optimum CDCA concentration (8 mM) is combined with the ZnO blocking layer in DSSC7 leading to the highest J_{sc} and V_{oc} of 3.09 mA/cm^2 and 0.66 V respectively and consequently best device performance. The highest recombination resistance is obtained for the cell with the blocking layer as the blocking layer prevents the injected electrons to come in direct contact with the electrolyte and consequently reduces the direct capture of electrons by the I_3^- ions of the electrolyte. Furthermore, the CDCA addition with optimum concentration and blocking layer increases the number of electrons accumulated in the conduction band of ZnO which led to increased electron density. This creates a small shift of Fermi level for the electrons present in the ZnO. This rise in Fermi level slightly improves V_{oc} which can also be observed from Table 5.1 [36,61].

Apart from recombination resistance, the second semicircle also provides information about the electron lifetime in the conduction band of ZnO which gives the measure of the rate at which the recombination reaction occurs. This lifetime is inversely proportional to the oscillation frequency at which the peak on the second arc is obtained. But, since, the frequency information is missing in the Nyquist plot; the electron lifetime can be calculated from the phase bode plot using the formula

$$\tau_e = \frac{1}{2\pi f_{peak}} \qquad (4)$$

where f_{peak} represents the peak frequency of phase Bode plot in the mid-frequency range as shown in Fig. 5.15(b). A shift in the peaks may be observed in the Bode plots of the DSSCs prepared following different procedures. Shifting of peak frequency towards lower frequency represents longer electron lifetime (τ_e) and slower recombination process. The calculated electron lifetimes for all the cells are summarised in Table 5.2. The highest electron lifetime of 24.35 ms is obtained for the cell fabricated with 8 mM CDCA concentration along with ZnO compact blocking layer (DSSC 7). The increased electron lifetime due to CDCA and blocking layer effectively enhances the photoconversion efficiency (PCE) which is in good agreement with the results obtained from J-V measurement. The reduced dye aggregation in presence of CDCA and inhibition of electron recombination by the blocking layer may be accounted for this.

5.4. Conclusion

Effects of co-adsorption of CDCA and ZnO blocking layer were investigated in Rose Bengal dye based DSSCs. The surface, photovoltaic and electrochemical properties of all the cells were extensively studied. The strong binding of CDCA molecules to the ZnO surface partially displaces dye molecules and consequently reduces photon harvesting. Excessive CDCA concentration implies significantly reduced dye attachment to the ZnO surface leading to decreased amount of light energy absorption. Therefore, to maximize the positive effect of the co-adsorbent, it is very crucial to carefully optimize the amount of CDCA. The amount of CDCA has been optimized by adjusting its concentration in the dye solution and found that the best device performance was obtained for 8 mM concentration. At optimized co-adsorbent concentration, the reduced dye loading due to the presence of CDCA and consequently decreased light-harvesting was compensated by the increased electron injection efficiency leading to maximum device efficiency of 1 %. The performance was further increased from 1.00 % to 1.22 % when a compact

ZnO blocking layer was added to the FTO before depositing the mesoporous ZnO active layer. This was due to the suppression of electron back transfer from the FTO to the liquid electrolyte. These results indicate that the addition of CDCA as a dye co-adsorbent and the introduction of ZnO blocking layer is an effective way to boost the performance of Rose Bengal dye based DSSCs. The efficiency of the fabricated cells is low as the dye used in this study is rose bengal. Though the efficiency is low here compared to the ruthenium based cells, it lies in the range of efficiency of rose bengal dye based DSSCs obtained by other researchers. Higher efficiencies can be obtained by using high performance ruthenium dye.

References:

[1] Bach, W.: Global warming: the complete briefing (2nd ed). John Houghton. Cambridge University Press: Cambridge, 1997. Pp. xv + 251. Paperback: ISBN 0521-62932-2, ??12.95; hardback: ISBN 0-321-62089-9, ??35.00. Int. J. Climatol. (1998). https://doi.org/10.1002/(sici)1097-0088(199804)18:5<579::aid-joc278>3.3.co;2-0

[2] Meadows, D.H., Meadows, D.L., Randers, J., Behrens, W.: The Limits to Growth - Club of Rome. (1972). http://www.donellameadows.org/wp-content/userfiles/Limits-to-Growth-digital-scan-version.pdf

[3] Hosenuzzaman, M., Rahim, N.A., Selvaraj, J., Hasanuzzaman, M., Malek, A.B.M.A., Nahar, A.: Global prospects, progress, policies, and environmental impact of solar photovoltaic power generation, 41, 284-297 (2015). https://doi.org/10.1016/j.rser.2014.08.046

[4] Barbir, F., Veziroğlu, T.N., Plass, H.J.: Environmental damage due to fossil fuels use. Int. J. Hydrogen Energy. 15(10), 739-749 (1990). https://doi.org/10.1016/0360-3199(90)90005-J

[5] Goetzberger, A., Hebling, C., Schock, H.W.: Photovoltaic materials, history, status and outlook. Materials Science and Engineering: R: Reports. 40(1), 1-46 (2003). https://doi.org/10.1016/S0927-796X(02)00092-X.

[6] Alharbi, F., Bass, J.D., Salhi, A., Alyamani, A., Kim, H.C., Miller, R.D.: Abundant non-toxic materials for thin film solar cells: Alternative to conventional materials. Renew. Energy. 36, 2753–2758 (2011).

[7] Lee, T.D., Ebong, A.U.: A review of thin film solar cell technologies and challenges, 70, 1286–1297 (2017). https://doi.org/10.1016/j.rser.2016.12.028

[8] Yamamoto, K., Yoshimi, M., Tawada, Y., Okamoto, Y., Nakajima, A.: Cost effective and high-performance thin film Si solar cell towards the 21st century. Sol. Energy Mater. Sol. Cells. 66, 117–125 (2001).

https://doi.org/10.1016/S0927-0248(00)00164-1

[9] O'Regan, B., Grätzel, M.: A low-cost, high-efficiency solar cell based on dye-sensitized colloidal TiO2 films. Nature. 353(6346), 737-740 (1991). https://doi.org/10.1038/353737a0

[10] Chiba, Y., Islam, A., Komiya, R., Koide, N., Han, L.: Conversion efficiency of 10.8% by a dye-sensitized solar cell using a TiO2 electrode with high haze. Appl. Phys. Lett. 88, 223505 (2006). https://doi.org/10.1063/1.2208920

[11] Grätzel, M.: Solar energy conversion by dye-sensitized photovoltaic cells. Inorg. Chem. 44(20), 6841-6851 (2005). https://doi.org/10.1021/ic0508371

[12] Chung, I., Lee, B., He, J., Chang, R.P.H., Kanatzidis, M.G.: All-solid-state dye-sensitized solar cells with high efficiency. Nature. 485(7399), 486-489 (2012). https://doi.org/10.1038/nature11067

[13] Cai, N., Moon, S.J., Cevey-Ha, L., Moehl, T., Humphry-Baker, R., Wang, P., Zakeeruddin, S.M., Grätzel, M.: An organic D-π-A dye for record efficiency solid-state sensitized heterojunction solar cells. Nano Lett. 11(4), 1452-1456 (2011). https://doi.org/10.1021/nl104034e

[14] Grätzel, M.: Dye-sensitized solar cells, J. Photochem. Photobiol. C Photochem. Rev. 4(2), 145-153 (2003). https://doi.org/10.1016/S1389-5567(03)00026-1.

[15] Shao, F., Sun, J., Gao, L., Yang, S., Luo, J.: Growth of various TiO2 nanostructures for dye-sensitized solar cells. J. Phys. Chem. C. 115(5), 1819-1823 (2011). https://doi.org/10.1021/jp110743m

[16] Tiwana, P., Docampo, P., Johnston, M.B., Snaith, H.J., Herz, L.M.: Electron mobility and injection dynamics in mesoporous ZnO, SnO 2, and TiO2 films used in dye-sensitized solar cells. ACS Nano. 5(6), 5158-5166 (2011). https://doi.org/10.1021/nn201243y

[17] Biswas, R., Chatterjee, S.: Effect of surface modification via sol-gel

spin coating of ZnO nanoparticles on the performance of WO3 photoanode based dye sensitized solar cells. Optik (Stuttg). 212, 164142 (2020). https://doi.org/10.1016/j.ijleo.2019.164142

[18] Zhang, Q., Dandeneau, C.S., Zhou, X., Cao, C.: ZnO nanostructures for dye-sensitized solar cells, 21(41), 4087-4108 (2009). https://doi.org/10.1002/adma.200803827

[19] Guillén, E., Peter, L.M., Anta, J.A.: Electron transport and recombination in ZnO-based dye-sensitized solar cells. J. Phys. Chem. C. 115(45), 22622-22632 (2011). https://doi.org/10.1021/jp206698t

[20] Quintana, M., Edvinsson, T., Hagfeldt, A., Boschloo, G.: Comparison of dye-sensitized ZnO and TiO2 solar cells: Studies of charge transport and carrier lifetime. J. Phys. Chem. C. 111(2), 1035-1041. (2007). https://doi.org/10.1021/jp065948f

[21] Vittal, R., Ho, K.C.: Zinc oxide based dye-sensitized solar cells: A review. Renew. Sustain. Energy Rev. 70, 920-935 (2017). https://doi.org/10.1016/j.rser.2016.11.273

[22] Biswas, R., Roy, T., Chatterjee, S.: Study of Electro-Optical Performance and Interfacial Charge Transfer Dynamics of Dye Sensitized Solar Cells Based on ZnO Nanostructures and Natural Dyes. J. Nanoelectron. Optoelectron. 14(1), 99-108 (2019). https://doi.org/10.1166/jno.2019.2445

[23] Ito, S., Nazeeruddin, M.K., Liska, P., Comte, P., Charvet, R., Péchy, P., Jirousek, M., Kay, A., Zakeeruddin, S.M. and Grätzel, M.: Photovoltaic characterization of dye-sensitized solar cells: effect of device masking on conversion efficiency. Progress in photovoltaics: research and applications, 14(7), pp.589-601 (2006). https://doi.org/10.1002/pip.683

[24] Aghazada, S. and Nazeeruddin, M.K.: Ruthenium complexes as sensitizers in dye-sensitized solar cells. Inorganics, 6(2), p.52 (2018). https://doi.org/10.3390/inorganics6020052

[25] Nazeeruddin, M.K., Baranoff, E. and Grätzel, M.: Dye-sensitized solar cells: a brief overview. Solar energy, 85(6), pp.1172-1178 (2011). https://doi.org/10.1016/j.solener.2011.01.018

[26] Sayyed, S.A., Beedri, N.I., Kadam, V.S. and Pathan, H.M.: Rose Bengal sensitized bilayered photoanode of nano-crystalline TiO2–CeO2 for dye-sensitized solar cell application. Applied Nanoscience, 6(6), pp.875-881 (2016). https://doi.org/10.1007/s13204-015-0495-6

[27] Pradhan, B., Batabyal, S.K. and Pal, A.J.: Vertically aligned ZnO nanowire arrays in Rose Bengal-based dye-sensitized solar cells. Solar energy materials and solar cells, 91(9), pp.769-773 (2007). https://doi.org/10.1016/j.solmat.2007.01.006

[28] Duffy, N.W., Peter, L.M., Rajapakse, R.M.G. and Wijayantha, K.G.U.: Investigation of the kinetics of the back reaction of electrons with tri-iodide in dye-sensitized nanocrystalline photovoltaic cells. The Journal of Physical Chemistry B, 104(38), pp.8916-8919 (2000). https://doi.org/10.1021/jp001185z

[29] Rani, S., Shishodia, P.K. and Mehra, R.M.: Enhancement of photovoltaic performance of quasi-solid state dye sensitized solar cell with dispersion of a hole conducting agent. Materials Science-Poland, 28(1), p.281 (2010).

[30] Kim, H., Veerappan, G., & Park, J. H.: Conducting polymer coated non-woven graphite fiber film for dye-sensitized solar cells: superior Pt-and FTO-free counter electrodes. Electrochimica Acta, 137, 164-168(2014). https://doi.org/10.1016/j.electacta.2014.06.012

[31] Patwari, J., Sardar, S., Liu, B., Lemmens, P., & Pal, S. K.: Three-in-one approach towards efficient organic dye-sensitized solar cells: aggregation suppression, panchromatic absorption and resonance energy transfer. Beilstein journal of nanotechnology, 8(1), 1705-1713(2017). https://doi.org/10.3762/bjnano.8.171

[32] Zhang, L., Cole, J.M.: Dye aggregation in dye-sensitized solar cells. J. Mater. Chem. A. 5(37), 19541-19559 (2017). https://doi.org/10.1039/c7ta05632j

[33] Buene, A.F., Almenningen, D.M., Hagfeldt, A., Gautun, O.R., Hoff, B.H.: First Report of Chenodeoxycholic Acid–Substituted Dyes Improving the Dye Monolayer Quality in Dye-Sensitized Solar Cells. Sol. RRL. 4(4), 1900569 (2020). https://doi.org/10.1002/solr.201900569

[34] Kumar, V., Gupta, R., Bansal, A.: Role of chenodeoxycholic acid as co-additive in improving the efficiency of DSSCs. Sol. Energy. 196, 589-596 (2020). https://doi.org/10.1016/j.solener.2019.12.034

[35] Ismail, M., Ahmad Ludin, N., Hisham Hamid, N., Adib Ibrahim, M., Sopian, K.: The Effect of Chenodeoxycholic Acid (CDCA) in Mangosteen (Garcinia mangostana) Pericarps Sensitizer for Dye-Sensitized Solar Cell (DSSC). In: Journal of Physics: Conference Series. Vol. 1083, No. 1, p. 012018 (2018). doi :10.1088/1742-6596/1083/1/012018

[36] Li, J., Wu, W., Yang, J., Tang, J., Long, Y., Hua, J.: Effect of chenodeoxycholic acid (CDCA) additive on phenothiazine dyes sensitized photovoltaic performance. Sci. China Chem. 54(4), 699-706 (2011). https://doi.org/10.1007/s11426-011-4227-9

[37] Inoue, T., Pandey, S. S., Fujikawa, N., Yamaguchi, Y., & Hayase, S.: Synthesis and characterization of squaric acid based NIR dyes for their application towards dye-sensitized solar cells. Journal of Photochemistry and Photobiology A: Chemistry, 213(1), 23-29(2010). https://doi.org/10.1016/j.jphotochem.2010.04.015

[38] Lee, K. M., Suryanarayanan, V., Ho, K. C., Thomas, K. J., & Lin, J. T.: Effects of co-adsorbate and additive on the performance of dye-sensitized solar cells: A photophysical study. Solar energy materials and

solar cells, 91(15-16), 1426-1431(2007). https://doi.org/10.1016/j.solmat.2007.03.009

[39] Yum, J. H., Jang, S. R., Humphry-Baker, R., Grätzel, M., Cid, J. J., Torres, T., & Nazeeruddin, M. K.: Effect of coadsorbent on the photovoltaic performance of zinc pthalocyanine-sensitized solar cells. Langmuir, 24(10), 5636-5640(2008). https://doi.org/10.1021/la800087q

[40] Lu, H. P., Tsai, C. Y., Yen, W. N., Hsieh, C. P., Lee, C. W., Yeh, C. Y., & Diau, E. W. G.: Control of dye aggregation and electron injection for highly efficient porphyrin sensitizers adsorbed on semiconductor films with varying ratios of coadsorbate. The Journal of Physical Chemistry C, 113(49), 20990-20997(2009). https://doi.org/10.1021/jp908100v

[41] Yang, Y., Peng, X., Chen, S., Lin, L., Zhang, B., Feng, Y.: Performance improvement of dye-sensitized solar cells by introducing a hierarchical compact layer involving ZnO and TiO2 blocking films. Ceram. Int. 40(9), 15199-15206 (2014). https://doi.org/10.1016/j.ceramint.2014.07.001

[42] Yeoh, M.E., Chan, K.Y.: Efficiency Enhancement in Dye-Sensitized Solar Cells with ZnO and TiO2 Blocking Layers. J. Electron. Mater. 48(7), 4342-4350 (2019). https://doi.org/10.1007/s11664-019-07207-5

[43] Wong, K.K., Ng, A., Chen, X.Y., Ng, Y.H., Leung, Y.H., Ho, K.H., Djurišić, A.B., Ng, A.M.C., Chan, W.K., Yu, L., Phillips, D.L.: Effect of ZnO nanoparticle properties on dye-sensitized solar cell performance. ACS Appl. Mater. Interfaces. 4(3), 1254-1261 (2012). https://doi.org/10.1021/am201424d

[44] Elilarassi, R., Chandrasekaran, G.: Effect of annealing on structural and optical properties of zinc oxide films. Mater. Chem. Phys. 121(1-2), 378-384 (2010). https://doi.org/10.1016/j.matchemphys.2010.01.053

[45] Shivaraj, B.W., Murthy, H.N.N., Krishna, M., Satyanarayana, B.S.: Effect of Annealing Temperature on Structural and Optical Properties of

Dip and Spin coated ZnO Thin Films. Procedia Mater. Sci. 10, 292-300 (2015). https://doi.org/10.1016/j.mspro.2015.06.053

[46] Al-Kahlout, A.: Thermal treatment optimization of ZnO nanoparticles-photoelectrodes for high photovoltaic performance of dye-sensitized solar cells. J. Assoc. Arab Univ. Basic Appl. Sci. 17(1), 66-72. (2015). https://doi.org/10.1016/j.jaubas.2014.02.004

[47] Pandey, P., Parra, M.R., Haque, F.Z., Kurchania, R.: Effects of annealing temperature optimization on the efficiency of ZnO nanoparticles photoanode based dye sensitized solar cells. J. Mater. Sci. Mater. Electron. 28(2), 1537-1545 (2017). https://doi.org/10.1007/s10854-016-5693-9

[48] AR SAYYED, S.A., Beedri, N.I., Kadam, V.S. and Pathan, H.M.: Rose bengal-sensitized nanocrystalline ceria photoanode for dye-sensitized solar cell application. Bulletin of Materials Science, 39(6), pp.1381-1387(2016). https://doi.org/10.1007/s12034-016-1279-7

[49] Ossai, A. N., Alabi, A. B., Ezike, S. C., & Aina, A. O. :Zinc oxide-based dye-sensitized solar cells using natural and synthetic sensitizers. Current Research in Green and Sustainable Chemistry, 3, 100043(2020). https://doi.org/10.1016/j.crgsc.2020.100043

[50] Henson, Z.B., Zhang, Y., Nguyen, T.Q., Seo, J.H. and Bazan, G.C.: Synthesis and properties of two cationic narrow band gap conjugated polyelectrolytes. Journal of the American Chemical Society, 135(11), pp.4163-4166 (2013). https://doi.org/10.1021/ja400140d

[51] Seo, D.K. and Hoffmann, R.: Direct and indirect band gap types in one-dimensional conjugated or stacked organic materials. Theoretical Chemistry Accounts, 102(1), pp.23-32 (1999). https://doi.org/10.1007/s002140050469

[52] Nguyen, W.H., Bailie, C.D., Burschka, J., Moehl, T., Grätzel, M., McGehee, M.D. and Sellinger, A.: Molecular engineering of organic

dyes for improved recombination lifetime in solid-state dye-sensitized solar cells. Chemistry of Materials, 25(9), pp.1519-1525 (2013). https://doi.org/10.1021/cm3036357

[53] Prima, E.C., Al Qibtiya, M., Yuliarto, B. and Dipojono, H.K.: Influence of anthocyanin co-pigment on electron transport and performance in black rice dye-sensitized solar cell. Ionics, 22(9), pp.1687-1697 (2016). https://doi.org/10.1007/s11581-016-1673-6

[54] Costantino, U., Marmottini, F., Nocchetti, M., Vivani, R.: New synthetic routes to hydrotalcite-like compounds - Characterisation and properties of the obtained materials. Eur. J. Inorg. Chem. 1998(10), 1439-1446 (1998). https://doi.org/10.1002/(sici)1099-0682(199810)1998:10<1439::aid-ejic1439>3.0.co;2-1

[55] Oh, J.M., Hwang, S.H., Choy, J.H.: The effect of synthetic conditions on tailoring the size of hydrotalcite particles. In: Solid State Ionics (2002)

[56] Liu, X., Zhang, Q., Li, J., Valanoor, N., Tang, X., Cao, G.: Increase of power conversion efficiency in dye-sensitized solar cells through ferroelectric substrate induced charge transport enhancement. Sci. Rep. 8(1), 1-8 (2018). https://doi.org/10.1038/s41598-018-35764-y

[57] Mazloum-Ardakani, M., & Arazi, R.: Improving the effective photovoltaic performance in dye-sensitized solar cells using an azobenzenecarboxylic acid-based system. Heliyon, 5(3), e01444(2019). https://doi.org/10.1016/j.heliyon.2019.e01444

[58] Zhao, Y., Lu, F., Zhang, J., Dong, Y., Zhang, B., & Feng, Y.: Stepwise co-sensitization of two metal-based sensitizers: probing their competitive adsorption for improving the photovoltaic performance of dye-sensitized solar cells. RSC advances, 7(17), 10494-10502(2017). https://doi.org/10.1039/C6RA28473F

[59] Ondersma, J.W., Hamann, T.W.: Impedance investigation of dye-sensitized solar cells employing outer-sphere redox shuttles. J. Phys. Chem. C. 114(1), 638-645 (2010). https://doi.org/10.1021/jp908442p

[60] Chou, J.C., Lu, C.C., Liao, Y.H., Lai, C.H., Nien, Y.H., Kuo, C.H., Ko, C.C.: Fabrication and Electrochemical Impedance Analysis of Dye-Sensitized Solar Cells with Titanium Dioxide Compact Layer and Graphene Oxide Dye Absorption Layer. IEEE Trans. Nanotechnol. 18, 461-466 (2019). https://doi.org/10.1109/TNANO.2019.2913537

[61] Wei, L., Yang, Y., Zhu, Z., Fan, R., Wang, P., Dong, Y., Chen, S.: Effect of different donor groups in bis(6-methoxylpyridin-2-yl) substituted co-sensitizer on the performance of N719 sensitized solar cells. RSC Adv. 5(117), 96934-96944 (2015). https://doi.org/10.1039/c5ra19417b